DOI: 10.1002/chem.200701223

Tailor-Made Poly(amidoamine)s for Controlled Complexation and Condensation of DNA

Laura Hartmann,[a] Stefanie Häfele,[b] Regine Peschka-Süss,[b] Markus Antonietti,[a] and Hans G. Börner*[a]

Abstract: A set of polymer carriers for DNA delivery was synthesized by combining monodisperse, sequence-defined poly(amidoamine) (PAA) segments with poly(ethylene oxide) (PEO) blocks. The precise definition of the PAA segments provides the possibility of correlating the chemical structure (monomer sequence) with the resulting biological properties. Three different PAA–PEO conjugates were synthesized by solid-phase supported synthesis, and the cationic nature of the PAA segments was systematically varied. This allows for the tailoring of interactions with double-stranded plasmid DNA (dsDNA). The potential of the PAA–PEO conjugates as non-viral vectors for gene delivery is demonstrated by investigating the dsDNA complexation and condensation properties. Depending on the applied carrier, a transition in polyplex (polymer–DNA ion complex) structures is observed. This reaches from extended ring-like structures to highly compact toroidal structures, where supercoiling of the DNA is induced. An aggregation model is proposed that is based on structural investigations of the polyplexes with atomic force microscopy (AFM) and dynamic light scattering (DLS). While the cationic PAA segment mediates primarily the contact of the carrier to the dsDNA, the PEO block stabilizes the polyplex and generates a "stealth" aggregate, as was suggested by Zeta potentials that were close to zero. The controlled aggregation leads to stable, single-plasmid complexes, and stabilizes the DNA structure itself. This is shown by ethidium bromide intercalation assays and DNase digestion assays. The presented PAA–PEO systems allow for the formation of well-defined single-plasmid polyplexes, preventing hard DNA compression and strongly polydisperse polyplexes. Moreover carrier polymers and the resulting polyplexes exhibit no cytotoxicity, as was shown by viability tests; this makes the carriers potentially suitable for in vivo delivery applications.

Keywords: DNA packing · drug delivery · gene delivery · peptidomimetics · polymers · polyplex

Introduction

New carrier systems for non-viral gene therapy are still a major issue in biomedical research. The use of DNA as a therapeutic drug offers enormous opportunities, particularly for the therapy of hereditary diseases as well as in new cancer and HIV therapies.[1,2] Nevertheless, so far the number of registered products for commercially available gene delivery is virtually zero, but better carriers and stabilizers would certainly contribute to the realization of a practicably therapeutic approach.[3] Next to viral vectors, which often exhibit high immunogenicity and unpredictable toxicity, the use of non-viral vectors that are based on polymer carriers offers enormous potential. Most of the polymeric vectors exhibit lower cytotoxicity, reduced hemotoxicity and much less immunogenicity compared to the viral vectors.[4] Despite all these advantages they still exhibit significantly lower transfection efficiencies. In recent years, many different polymers were studied as non-viral vectors. However, the mechanisms of active transport and release are still very poorly understood; this makes it very difficult to design new polymeric carriers for this purpose.[5–7]

Currently, branched poly(ethyleneimine)s (PEIs) are known as the reference standard of non-viral vectors for

[a] Dr. L. Hartmann, Prof. Dr. M. Antonietti, Dr. H. G. Börner
Max Planck Institute of Colloids and Interfaces
Department of Colloid Chemistry, MPI KG Golm
14424 Potsdam (Germany)
Fax: (+49) 331-567-9502
E-mail: hans.boerner@mpikg.mpg.de

[b] Dr. S. Häfele, Prof. Dr. R. Peschka-Süss
Albert-Ludwigs-University Freiburg
Department of Pharmaceutical Technology and Biopharmacy
Stefan-Meier-Strasse 19
79104 Freiburg i. Br. (Germany)

Supporting information for this article is available on the WWW under http://www.chemeurj.org/ or from the author.

gene therapy, because they show high transfection efficiencies.[7,8] Nevertheless PEI suffers from major limitations as a non-viral vector, for example, like most polycations, it is cytotoxic.[9] Furthermore, PEI is molecularly and chemically rather ill-defined, because of its broad distribution in both molecular weight and topology (branching).[10] These polydispersities strongly influence the number, type and distribution of cationic charges, which thereby are different for every polymer macromolecule.[10,11] Because these properties are of an enormous relevance to the DNA complexation properties, the cell surface interactions, as well as the toxicity of the system, a direct correlation between the chemical structure of the polymer and its resulting biological properties is quite complicated. The strong impact of structural polydispersity was shown for PEI polyplexes (PEI–DNA ion-complexes) that were purified by chromatographic techniques, which separate the polyplexes from free, low-molecular-weight PEI. The purified polyplexes showed a strongly reduced cytotoxicity, but also a dramatic decrease in transfection efficiency; this indicates the importance of the low-molecular-weight PEI fraction for both cell internalization as well as toxicity.[12]

Therefore, highly defined macromolecules with sharply defined structure–property relationships are required, in order to correlate polymer properties with the resulting effects in biological systems. So far, dendrimers as monodisperse macromolecules offer the most precise chemical structure and are already in use for several drug-delivery applications.[13] Even though numerous functionalities can be incorporated, dendrimers are limited in their structure. Frequently, they exhibit globular structures, which can either keep the drug bound inside in a container-like fashion, or the functionalities on the periphery could be used, for example, for DNA complexation.[14]

So far only nature itself realizes the combination of a multifunctional monodisperse system with precise self-assembly to design a multitude of functional structures. Peptides and proteins are the most prominent examples. They are assembled by a limited number of amino acid building blocks, which bear different functionalities. The sequence of these amino acids within a linear chain then determines the resulting properties, for example, structure, solubility and charges. Biopolymers such as proteins and related peptide–polymer conjugates[15] certainly have a great potential for biomedical applications, but again, they are strongly limited due to their propensity for inducing immunogenic responses (peptides or proteins are simply too well known to the organism).[1,6] Therefore, it would be highly interesting to combine the advantages of both the precise structural and functional definition of peptides with the broad chemical variability of synthetic polymers.

A new approach towards monodisperse, multifunctional poly(amidoamine)s (PAAs) was presented earlier.[16] The route involved fully automated, solid-phase supported synthesis techniques, combined with protecting group strategies. This allowed for the sequential assembly of functional monomers to linear PAA segments. Monodisperse PAAs with monomer sequence control could be accessed, thus making the precise positioning of different functionalities along the PAA chain possible.[17] Because the synthesis of PAAs still remains compatible with the solid-phase supported synthesis of peptides, it was possible to fully automate the PAA synthesis. Furthermore, the use of PEO-attached polystyrene resins (PAP) or peptide-preloaded resins easily leads to PEO–PAA or peptide–PAA conjugates.[18,19]

Here, we present a set of PEO-*block*-PAA conjugates that were designed as polymeric carrier systems for gene delivery. PAAs are already known for their excellent biocompatibility and low cytotoxicity.[20] A monodisperse, sequence-defined PAA segment in combination with a PEO block should provide tuneable carriers with high potential for in vivo and in vitro applications.[21] The possibility of defining the monomer sequence of the PAA segment enables one to position cationic functionalities precisely within the PAA chain. The precise definition of the properties of the functional PAA segment might allow the correlation between the chemical structure of the carrier and the resulting properties, for instance, the DNA complexation ability.

Results and Discussion

A set of PEO–PAA conjugates was synthesized. The polymers always contain the same PEO block ($M_n = 2700$; $M_w/M_n = 1.06$) but differ in the cationic functionalities within the PAA segments. The synthesis of the PAA segment was accomplished by using solid-phase supported synthesis and a stepwise addition of diamine and dicarboxylic building blocks. Because the chemistry of these addition reactions is compatible with the classical protocols of the Merrifield solid-phase supported peptide synthesis, the assembly of the PAA segment can be easily automated by using a common peptide synthesizer. Furthermore, this enlarges the "monomer alphabet" that is available for PAA synthesis by the α-amino acids, and enables the introduction of single amino acids or peptide sequences within the PAA segment.

To investigate the influence of the monomer sequence of the PAA segment on its ability to interact with DNA, different cationic characters were implemented into the PAA segments by introducing functional building blocks that differ in their cationic functionalities, such as tertiary, secondary and primary amines (see Scheme 1). Branched PEI, the current reference carrier for gene delivery, also exhibits a mixture of these three functionalities, which strongly differ in their basicity and their ability to form hydrogen bonds. Other polymeric carrier systems mostly expose only one sort of cationic functionality, for example, primary amines for poly-(L-lysine), secondary amines for linear PEI, or tertiary amines for PAA dendrimers. Studies on the relationship between the chemical structure of PEI and its transfection efficiency give strong evidence that especially the combination of these three different cationic functionalities plays an important role in the gene transfection process.[10,22]

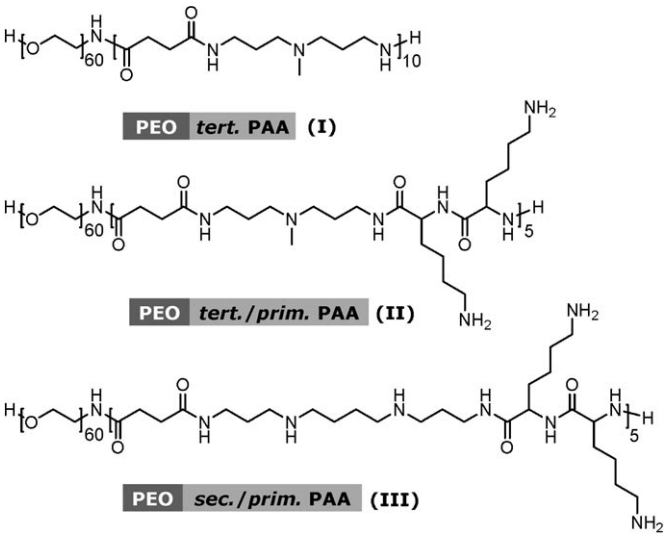

Scheme 1. Chemical structures of the PEO-*block*-PAA conjugates that bear only tertiary (PEO–*t*PAA), **I**), tertiary and primary (PEO–*tp*PAA, **II**) or secondary and primary amines (PEO–*sp*PAA, **III**) within the PAA segment.

To investigate these complex effects more systematically, PAA segments were designed that exhibit different combinations of the three amine functionalities (Scheme 1). A first PAA segment only features tertiary amines (PEO–*t*PAA, **I**). In a second system, these functionalities are complimented with primary amines by introducing lysines (PEO–*tp*PAA, **II**). In order to further increase the cationic strength of the PAA segment, the tertiary amines are replaced by secondary amines (PEO–*sp*PAA, **III**) in a third sample. All three of the presented PAA segments are linked to a PEO block to improve solubility and shielding. Most importantly for in vivo or in vitro experiments, the PEO provides the final polymer–DNA complexes with strong stabilization against aggregation with proteins or blood serum components. It is already known that conjugation with PEO increases the blood circulation time dramatically, and offers effective protection against undesired aggregation. After synthesis, the chemical structures of the PAA–PEO conjugates were confirmed consistently by NMR spectroscopy and mass spectrometry (see Experimental Section).

Polyplex (polyion complex) formation commonly is performed by mixing a solution of cationic polymer with a solution of DNA. In this study, experiments were carried out by using plasmid DNA (a closed ring of double-stranded DNA (dsDNA)) that encodes for the production of a green fluorescent protein (GFP) reporter, and represents a standard for transfection experiments. The resulting polyplex structures strongly depended on the exact protocol of mixing, that is, on the concentrations, volumes and mixing rates. The formation of an ion complex between two highly charged species (polyanions and polycations), usually is a rather rapid process. After the formation of the polyion complex upon the first contact of the two species, almost no rearrangements occur, and the polyplex stays in the kinetically controlled state. Because this first contact has such a strong influence on the formed structure, there is an enormous difference if the DNA is added to the polymer or vice versa. In one case, the polymer will bind to the DNA until charge compensation is achieved, in the other case, complex formation will strongly differ with time as the concentration of unbound polymer decreases. It is noteworthy that minor differences in mixing protocols often prevent the comparability of results from different laboratories. To ensure reproducible polyplex formation, a microfluidic device was used, which is referred to as a microfluidizer (see Supporting Information).[23] This microfluidizer consists of a Y-shaped channel system. The two arms of the channel have a width of 200 μm that unite into a channel with a width of 400 μm. This allows for the non-turbulent mixing of two solutions at a defined interface. Due to the design of the channel, mixing only occurs throughout diffusion at the interface (see Supporting Information). All polyplexes that have been characterized in this work were prepared by using a microfluidizer, which guarantees the high comparability of the results.

The complexation of dsDNA with multivalent polycations usually leads to the formation polyplexes with more compact structures. This process has been reported in the literature as the condensation of dsDNA.[24,25] Due to electrostatic repulsion of the negatively charged phosphate groups along the DNA backbone, the dsDNA is rather stiff, with persistence lengths of about 60 nm. Ion complex formation with a polycation reduces these repulsive forces, thus the dsDNA becomes more flexible, which results in bending and coiling.[24,26] This condensation process is highly important for the applicability of polyplexes for controlled DNA transport. As far as the mechanisms of cellular uptake are understood, effective translocation of a carrier system mainly depends on its size and charge. Condensing the DNA with a polycation to a complex with a size of around 100–500 nm and a cationic net charge is regarded to be favorable because it improves interactions with the cell membrane and stimulates the uptake.[27]

In order to investigate the ability of the different PEO–PAA conjugates to condense plasmid dsDNA, atomic force microscopy (AFM) measurements were performed. The ratio of polymer to DNA that was used for these samples was chosen according to the literature. Usually this ratio is expressed as the N/P ratio, the number of amine groups from the polymer (N) over the number of phosphate groups from the DNA backbone (P). For PAA-based systems, an N/P ratio of 10:1 is known to enable effective polyplex formation.[28]

The polyplexes that are formed by the three different PEO–PAA conjugates strongly differ from those that were prepared under the same conditions with PEI. For the PEO–PAA conjugate, the dsDNA is still recognizable, while the PEI polyplexes show undefined globular structures (Figure 1a and b–d). Within the series of the PEO-*block*-PAA carriers, there is a clear dependence of the polyplex structure on the cationic character of the PAA segment. These evident differences reveal a strong structure–property rela-

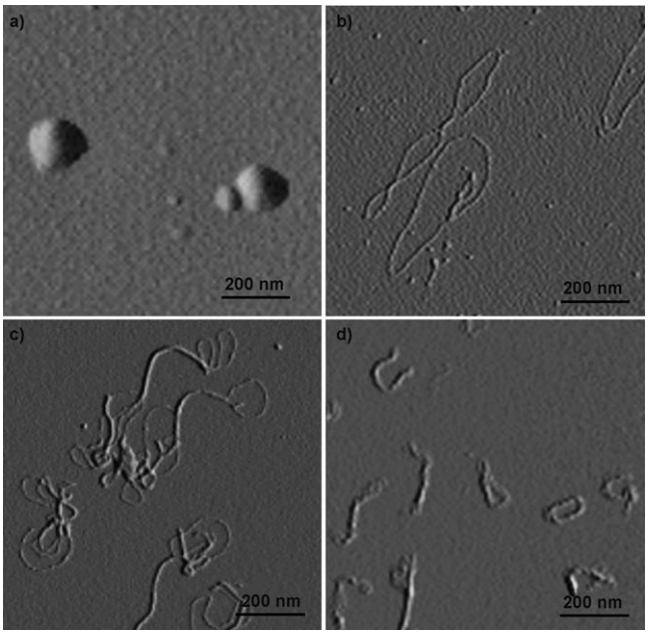

Figure 1. AFM images (phase-imaging mode) of polyplexes that are formed by plasmid dsDNA and PEI (a), PEO–*t*PAA (b), PEO–*tp*PAA (c), PEO–*sp*PAA (d) on mica. All polyplexes were prepared at an N/P ratio of 10:1 by using the microfluidizer.

tionship that can be more precisely interpreted now, due to the highly defined polymer structure.

The polyplex that is formed with the PEO–PAA conjugate that only bears tertiary amine groups (PEO–*t*PAA), shows the formation of expanded, ring-like structures on the AFM micrograph (Figure 1b). The adsorption of the structures on the negatively charged mica suggests that polyplex formation has taken place because adsorption requires a cationic net charge. In contrast to this, uncomplexed DNA cannot be visualized with this resolution on mica substrate; this is due to negative surface charges of mica, which prevents the strong adsorption of DNA. This was evident in control experiments, where a solution of non-complexed dsDNA was spin coated onto mica. AFM did not provide evidence for deposited structures, either because of the repulsive interactions between DNA and mica or because of the high mobility of the DNA on the substrate. Zeta potential measurements confirm the polyplex formation between the PEO–*t*PAA carrier and the dsDNA, because the complexes show an effective charge of around zero. This is expected and demonstrates that the plane-of-shear that is sensed with the electrophoresis measurements is far out from any ionic structure. Hence, the complex is effectively sterically shielded by the conjugated PEO chains. The original DNA plasmids that were measured under similar conditions reveal a strongly negative potential.

Taking these observations into account, a structure model can be suggested. Classical polycations, which are used as non-viral vectors such as PEI or PLL possess a large number of cationic functionalities, and thus, they complex DNA under condensation to a compact, globular entity with hard cationic surface charges (Scheme 2a). Frequent cross-linking of multiple plasmids is observed and is caused by kinetically controlled complexation processes.

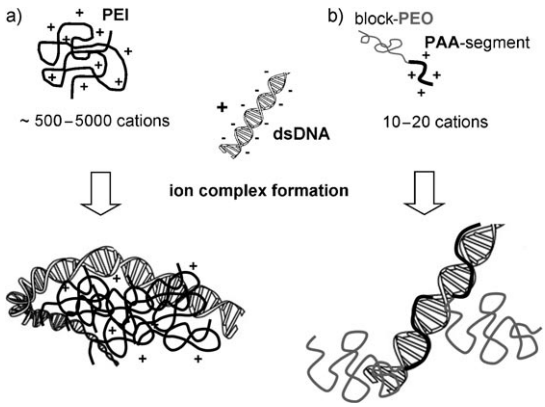

Scheme 2. Proposed model for the polyplex formation of PEI (a), and PEO–PAA conjugates (b) with double stranded DNA (dsDNA).

In contrast to this hard compression mode, the PEO–PAA conjugates only jacket the dsDNA because the small cationic segment can probably adapt to the DNA double helix structure without bridging or cross-linking. This process is regulated additionally by the PEO block that surrounds the formed complex, and shields the inner structure of the polyplex (Scheme 2b). This contributes to both the steric stabilization of the polyplexes and the shielding of the polyplex net charge, which are important properties for biomedical applications.

Light scattering (LS) proves that the structures that are observed with AFM correspond indeed to the solution structures. The polyplex that is formed with PEO–*t*PAA shows two species with hydrodynamic radii of 56 and 800 nm with $R_g/R_h \approx 1$; this indicates compacted, branched aggregates. The signal that corresponds to the smaller aggregates exhibits a higher intensity, and suggests the existence of single-plasmid complexes. The larger species however could be assigned to multi-plasmid aggregates. Because scattering is proportional to the square of the molecular weight, it can also be deduced that the majority of dsDNA probably forms single-plasmid complexes. For these experiments, an N/P ratio of 10:1 was used, but LS shows that structures that were formed at N/P ratios from 5:1 to 25:1 practically do not differ from the structures that are discussed above. According to the suggested jacketing model, the formation of open ring-like polyplexes points to the fact that the DNA helix is still too stiff for bending. Obviously, the complexation with tertiary amines cannot induce local conformational changes. The jacketing then will even support the structural persistence, presumably compensating the screening of electrostatic forces via steric repulsion. This is not desirable for biomedical applications because the translocation of rings is difficult.

The second PEO-*block*-PAA system introduces additional primary amines. These were positioned between the tertiary amines, and increase the number of amine functionalities in the PAA segment from ten to fifteen (Scheme 1). AFM measurements of the resulting polyplexes show supercoiled plasmid rings, which form multimeric bundles or rod-like structures (Figure 1c). Obviously, binding of the PAA segment provides the double helix with enough flexibility to allow for conformational changes, which results in the formation of compact supercoils (coil/coil). The PEO block probably still surrounds the formed structures, as can be assumed from the Zeta potentials, which are close to zero; this indicates a steric shielding of the PEO block. Light scattering of these structures in solution shows a hydrodynamic radius of 73 nm and $R_g/R_h \approx 1.9$, which suggests more anisotropic structures with a weak rod-like character. The onset of rod formation is evident in Figure 1c and confirms the LS data. It remains an open question (and more a question of cell physiology) if such multiplasmid polyplexes result in an improved polyplex uptake or not. Within the scope of the present study, it is concluded that the polyplex formation leads to less uniform structures, showing aggregation and a partial multimerization of the complexed dsDNA.

The third PAA segment with an even more increased ability for complexation is composed of primary and secondary amines (the latter replaces the tertiary amines of PEO–*tp*PAA (**II**)). Additionally, the number of amines was increased to twenty per PAA segment. AFM measurements show the formation of uniform, single-plasmid toroids (Figure 1d) and supercoiled dsDNA (Figure 2), as they are already known for highly effective polyplex formation.[29]

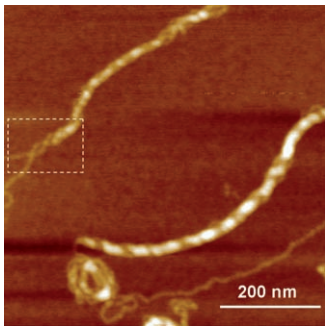

Figure 2. Induction of DNA supercoiling by defined interactions between the PEO–*sp*PAA carrier and plasmid DNA. The rod-like structures are formed by supercoiling of the DNA double helix. The on-going process of coil formation can be seen in the marked region, where two double strands of the plasmid form a supercoiled rod-like structure (AFM micrograph (height image) of the polyplexes, prepared via microfluidizer techniques).

The superhelix formation that is induced by distinct interactions of the DNA and the cationic carrier is now even perfected. The secondary rod-like supercoils then start bending to form more compact tertiary ring-like structures, which are referred to as toroids in the literature. Light-scattering investigations prove that these structures are also dominant in solution, with a hydrodynamic radius of 77 nm and a rod-like local structure, which is indicated by a plateau in the Holzer plot (see Supporting Information section). Such compact structures are highly desired for delivery purposes, because compression is very effective and cooperative unpacking might be possible.

After investigating the colloidal structure of the polyplexes that are formed with the different PEO–PAA conjugates, the fine structure of the DNA packing can be analyzed by using the ethidium bromide assay. The fluorescence dye (ethidium bromide) is a minor-groove intercalator and binds to undisturbed DNA double strands; this causes an increase of fluorescence due to the protection of the dye from solution quenching. If the complexation of the DNA with a polycation leads to a distortion of the double helix, the intercalation is disturbed, which results in an ejection of the fluorescent probe, and hence, a decrease in the fluorescence. The relative decrease of fluorescence is therefore often discussed as an indication for the strength of the condensation that is induced during polyplex formation. Chemically however, it is an indication for hard compression modes, which are caused by the contact with the carrier. As expected, the complexation of plasmid with PEI leads to a decrease in fluorescence; the DNA structure is slightly perturbed by the strongly bound PEI (Figure 3). In contrast to this, the complexation of the plasmid with the PEO–PAA conjugates results in an increase of the fluorescence. Given the proposed model of jacketing the dsDNA by the PEO–PAA conjugates, this can be explained by an increase of protection of the intercalated dye from quencher molecules, and might reflect the stabilization of the DNA helix by the carrier. Due to electrostatic repulsions, it appears to be not very likely that the increase of the fluorescence is caused by interactions between the ethidium bromide dye (a trivalent cation) and free carrier polymers. This was also demonstrated by a

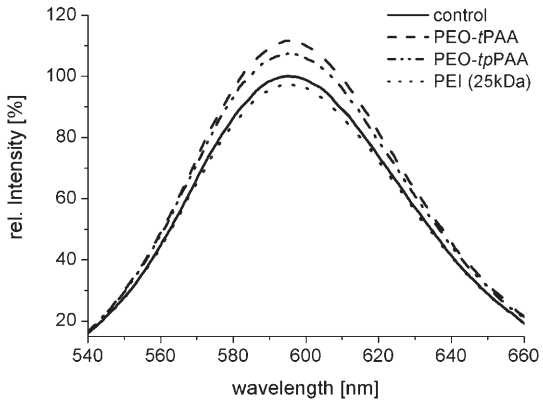

Figure 3. Ethidium bromide fluorescence assay of polyplexes formed with PEI, PEO–*t*PAA, and PEO–*tp*PAA. Ethidium bromide was added to a plasmid solution in buffer, incubated for 20 min, followed by standard polyplex preparation (microfluidizer, N/P 10:1). The fluorescence intensity was normalized to the control experiment (DNA + ethidium bromide), where no carrier polymer was added.

corresponding control experiment, where PEO-*block*-PAA was mixed with ethidium bromide (data not shown).

The shielding properties of the PEO–PAA conjugates are highly interesting with respect to in vitro and in vivo applications of the polyplexes. During transport through the organism, the polyplex has to be stabilized against disassembly. The resistance of polyplexes to enzymatic digestion can be investigated with a DNase assay and gel electrophoresis experiments. DNase is added to the sample after polyplex formation, where it digests accessible dsDNA. The migration behavior of the untreated and digested polyplexes is then monitored by gel electrophoresis. DNase is an enzyme that causes rapid digestion of unprotected DNA. This was demonstrated in Figure 4 (2nd and columns marked with DNA), where untreated plasmid results in a single, well-defined band (Figure 4, DNA (−)). The addition of DNase leads to the complete digestion of the DNA, and no sample band can be detected (Figure 4, DNA (*digest.*)). A poor shielding of the DNA by the polymer could also lead to complete digestion of the DNA cargo, whereas a favorable steric shielding of the polymer could inhibit or reduce the DNA degradation. Figure 4 shows the experiments for PEO–*t*PAA (left) and PEO–*sp*PAA (right). PEO–*t*PAA enables one to form polyplexes by starting at an N/P ratio of 5:1, as indicated by a retardation of the band. This is due to two facts: on the one hand, the mass of the polyplex is growing by ongoing complexation of polymer to the DNA. On the other hand, the net charge of the polyplex in comparison to the free plasmid is reduced due to charge compensation of the negative DNA backbone with the cationic PAA segments. By using an excess of polymer, polyplex formation can even lead to a charge reversal, which would result in a cationic net charge of the polyplex. These changes of the net charge would strongly slow down or completely suppress the movement of the sample band towards the cathode. The stronger retardation of the sample band for the PEO–*t*PAA conjugate at an N/P ratio of 10:1 therefore indicated a higher charge compensation compared to smaller N/P ratios. Nevertheless, even at high N/P ratios, there is only poor stabilization against enzymatic degradation with this polymer, as indicated by comparing the bands after treatment with DNase (see Figure 4). Enzymatic degradation is slightly reduced, but cannot be suppressed completely.

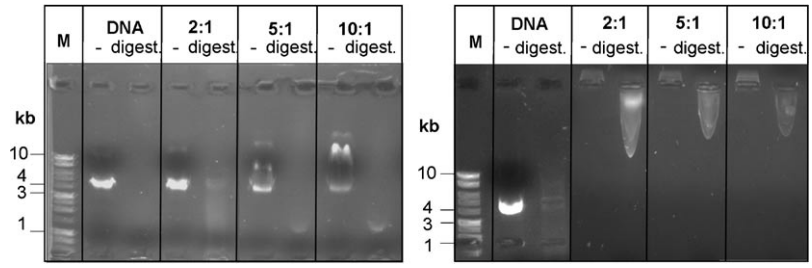

Figure 4. Gel electrophoresis experiments that show polyplex formation depending on the N/P ratio for PEO–*t*PAA (left) and PEO–*sp*PAA (right) as well as the stability of polyplexes against enzymatically digestion. Polyplexes were prepared by using the microfluidizer technique at different N/P ratios, and then were applied to gel electrophoresis (columns marked with: (−)). To test for the stability against enzymatic degradation, polyplexes were subsequently incubated with DNase (37 °C, 15 min.) and then applied to gel electrophoresis (columns marked with: *digest.*). Gel electrophoresis conditions: standard agarose gel (0.8 %) stained with ethidium bromide (100 mV, 45 min.).

The PEO–*sp*PAA conjugate shows strong polyplex formation already at an N/P ratio of 2:1. At all of the tested N/P ratios, the band of the polyplex remains at the starting point of the gel, which indicates a strong polyplex formation as well as the absence of negative net charges. The polyplex samples that were treated with DNase showed bands at a decreased molecular weight, but that still can be considered to be polyplexes. No bands for uncomplexed DNA or DNA fragments can be observed. Thus, the polymer seems to effectively shield the DNA against degradation and preserve the polyplex character even in the presence of strongly degrading enzymes.

For potential in vitro, and even more importantly in vivo delivery applications, an essential test has to be performed to investigate the toxicity of the systems. A luciferase assay was used to study the viability of the cells after contact with the different carriers and polyplexes. With this test, not only are dead cells detected, but also cells that are suffering from induced stress, for example, due to cell internalization of foreign substances can also be detected. Neither of the polymer carriers, nor the corresponding polyplexes showed an inherent cytotoxicity (Figure 5). In contrast to PEI, which causes an obvious decrease in cell viability, the PEO–PAA conjugates only stimulate a small increase in cell activity. This effect can be attributed to the translocation process that includes the internalization of the polymers and polyplexes, which

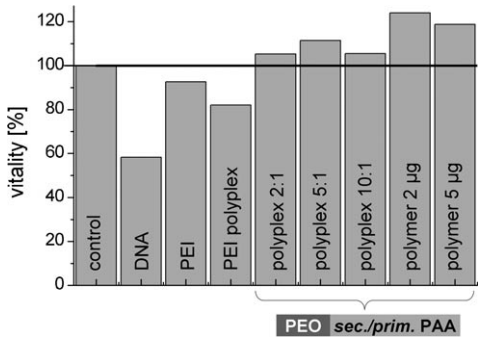

Figure 5. Viability assay for the PEO-*block*-PAA polymer and polyplexes compared to PEI. Cell viability was determined on COS7 cell lines by quantitative analysis of the amount of ATP by using a luciferase assay.

stimulates the metabolism of the cells but does not causes cell death.

Conclusion

In summary, an approach to the rational design of polymeric carriers for DNA delivery is presented. Three different poly(ethylene oxide-*block*-amidoamine) conjugates (PEO-*block*-PAA) were synthesized by using solid-phase supported synthesis. The polymers exhibited monodisperse PAA segments with systematically altered monomer sequences that are attached to a PEO block, which was kept constant. The choice of building blocks that are used to assemble the PAA segment allows for the precise positioning of amine functionalities with various base strengths. Thus, the cationic character could be precisely tuned by introducing tertiary, secondary and primary amine groups at specific sequence positions.

The polymeric carriers exhibit sharply defined sequence–property relationships that enabled us to correlate the polymeric structure with the DNA-interaction properties. The potentials of this PEO–PAA conjugates as non-viral vectors for gene delivery were demonstrated by investigating the complexation and compaction behavior with double-stranded plasmid DNA (dsDNA). The monodisperse nature of the functional PAA segment and the applied micro-fluidic mixing techniques result in highly reproducible dsDNA–polymer ion complexes (polyplexes). A strong influence of the cationic character of the PAA segments on the polyplex structures was apparent. In contrast to the usually applied branched poly(ethyleneimine), which results in ill-defined, globular, multi-plasmid polyplexes, the PEO–PAA conjugates lead to highly defined, single-plasmid complexes. Their structure hereby strongly depends on the cationic character that is encoded by the number and type of cationic functionalities within the PAA segment. This allowed us to control the polyplex structure; for instance, extended ring-like polyplexes were obtained if carriers with tertiary amines were used, and more condensed polyplexes were obtained by applying a carrier with a combination of tertiary and primary amines, whereas strongly compacted polyplexes were obtained in the case of carriers with combined secondary and primary amines. The latter carrier even exhibited a well-defined mode of compaction, as "super coiling" of the DNA cargo could be induced. The conjugate that combines secondary and primary amine moieties is certainly the most promising candidate for further biological analysis. It not only realizes highly condensed polyplexes, which are highly favourable for transport and cellular uptake, but also provides excellent stabilization against enzymatic DNA degradation, as was shown by DNase assays and gel electrophoresis.

A model was proposed that explains the complexation and condensation properties of the PEO-*block*-PAA conjugates: the cationic PAA-segment binds to the dsDNA and screens the negative charges of the DNA backbone, while the PEO block stabilizes the polyplex, and simultaneously produces "stealth" aggregates. This not only leads to stable single-plasmid complexes, but it even stabilizes the dsDNA structure itself, as was demonstrated by the intercalation of a fluorescent dye into the DNA double helix. Such a soft, stabilizing compression mode is of great importance for in vitro and in vivo applications, and cooperative unpacking of the cargo DNA at the desired location of action might be realizable, and would thus increase the effectiveness of the delivery system. Detailed transfection studies are currently on-going and will be reported elsewhere.

Experimental Section

Materials: Succinic acid anhydride (Suc, Aldrich, 99%), 3,3′-diamino-*N*-methyl-dipropylamine (Damp, Aldrich, 96%), spermine (Spe, Aldrich, 99%,), N^2,N^3-bis(*tert*-butoxycarbonyl-anhydride (tBoc$_2$O, IRIS Biotech GmbH, Marktredwitz, Germany), diisopropylethylamine (Acros, peptide grade), trifluoracetic acid (TFA; Acros, peptide grade), 1-benzotriazoyl-oxy-tris(pyrrolidino)-phosphonium hexafluorophosphate (PyBOP, Nova Biochem, Darmstadt, Germany) and 1-hydroxybenztriazol (HOBt, IRIS Biotech GmbH) were used as received. All other reagents were used as received from Aldrich. Fmoc-protected amino acid derivatives (Fmoc-Lys(Boc)OH), 2-(1*H*-benzotriazole-1-yl)-1,1,3,3-tetramethyluronium hexafluorophosphate (HBTU), *N*-methyl-2-pyrrolidone (NMP, 99.9+%, peptide synthesis grade) were used as received from IRIS Biotech GmbH (Marktredwitz, Germany). Dichloromethane (IRIS Biotech GmbH, peptide grade) was distilled from CaH_2 and *N*,*N*-dimethylformamide (DMF; Aldrich, 99+%) was distilled prior to use. Hydroxymethyl-phenoxy (Wang) PEO-attached peptide resin (Wang PAP) (loading: 0.27 mmol g^{-1}; $M_n = 2700$, $M_w/M_n = 1.06$ (GPC (THF, calibrated against linear PEO standards, PSS, Germany)) was synthesized as described previously.[18]

Instrumentation: The synthesis of the poly(amidoamine)s was performed on a fully automated ABI 433a peptide synthesizer by Applied Biosystems, Foster City CA, USA. Matrix-assisted laser desorption ionization time of flight mass spectrometry (MALDI-TOF-MS) measurements were performed on a Voyager-DE STR BioSpectrometry Workstation MALDI-TOF mass spectrometer (Perseptive Biosystems, Inc., Framingham, MA, USA). The samples were dissolved at concentrations of 0.1 mg mL^{-1} in MeOH. The analyte solution (1 μL) was mixed with α-cyano-4-hydroxycinnamic acid matrix solution (1 μL) that consisted of matrix (10 mg) that was dissolved in 0.1% TFA (1 mL) in acetonitrile/H_2O (1:1, *v*/*v*). The resulting mixture (1 μL) was applied to the sample plate. Samples were air-dried at ambient temperature. Measurements were performed at an acceleration voltage of 20 kV. Each obtained spectrum was the mean of 250 laser shots. The electrospray mass spectrometry (ESI) measurements were performed with N_2 (4.5 L min^{-1}) in the positive modus with a detector voltage of 1.6 kV, the injector temperature at 150 °C and a voltage of 4.5 kV. Nuclear magnetic resonance spectra (NMR) were recorded on a Bruker DPX-400 Spectrometer at 400.1 MHz. Dynamic light scattering measurements were performed on a goniometer with temperature control (±0.05 K), a photomultiplier and a multiple-tau digital correlator (ALV 500, ALV, Langen, Germany). A helium–neon laser at $\lambda = 633$ nm by Polytec, Waldbronn, Germany (PL 3000) with 34 mW performance was used. The measured correlation functions were evaluated with contin.[30] Parallel to the dynamic light scattering, static light scattering was measured on the same samples to obtain the R_g/R_h ratios. Cylindrical cuvettes (d = 1 cm) were cleaned with Hellmanex solution by using an ultrasonic bath and then were washed several times with millipore water. After rinsing the cuvettes with distilled acetone for 10 min, they were stored in a dust-free desiccator until use.

Zeta potential measurements: Samples were prepared according to standard protocols by using the microfluidic interfacial mixing at a DNA concentration of 0.5 mg mL^{-1} in Hepes buffer. Zeta-potential measurements

were carried out in the standard capillary electrophoresis cell of the Zetasizer 3000 HS from Malvern Instruments (Worcester, UK) at 25 °C. Sampling time was set to automatic and the average values were calculated with the data from three independent measurements (five runs each) of all samples. Atomic force microscopy (AFM) was performed on a NanoScope IIIa device (Veeco Instruments, Santa Barbara, CA) in tapping mode. Commercial silicon tips (Type NCR-W) were used with a tip radius <10 nm and a spring constant of 42 N m^{-1} at a resonance frequency of 285 kHz. The image was recorded on a 10×10 μm e^{-} scanner. The samples were prepared by dropping a 0.05 mg mL^{-1} DNA polyplex solution (5 μL) onto a freshly cleaved mica substrate. After 30 s adsorption and equilibration time, the samples were dried by rotating the substrate at 3000 rpm. The luminescent signal of the cell viability testing solutions was measured on a MicroLumat Plus LB 96 V Luminometer by EG&amp (G. Berthold, Bad Wildbad, Germany). The fluorescence measurements were performed in expendable plastic cuvettes at a luminometer by Perkin Elmer (Waltham MA, USA). Gel electrophoresis was performed on standard gel electrophoresis set-up by Biometra (Göttingen, Germany).

General synthesis of poly((ethylene oxide)-*block*-(amidoamine) conjugates (PEO–PAA conjugates): The monodisperse, sequence-defined PAA segments were prepared via a solid-phase supported synthesis as reported previously. In contrast to the classical solid-phase peptide synthesis (SPPS), which is based on Merrifield by using the stepwise addition of amino acids, the PAA segments were synthesized by a stepwise assembly of dicarboxylate and diamine building blocks. Therefore in a first step, a dicarboxylate building block that was activated as succinic anhydride (Suc) was coupled to a resin-bound amino group. Quantitative conversion was controlled via colorimetric tests and mass spectrometry. The subsequent coupling of a diamine building block was facilitated by PyBOP/HOBt/iPr$_2$NEt. Quantitative conversion was verified by colorimetric tests and mass spectrometry. The repetitive coupling of dicarboxylate and diamine building blocks by following these protocols led to monodisperse PAA segments with defined monomer sequences. To vary the functionalities within the PAA sequence different diamine building blocks can be used. For the introduction of tertiary amine groups 3,3-diamino-*N*-methyl-dipropylamine (Damp) was used. For the incorporation of secondary amine groups a spermine (Spe) derivative was synthesized that bore the *tert*-butyloxycarbonyl (*t*Boc) protective groups at the secondary amine functionalities. Side-groups of the building blocks had to be protected during the addition to avoid side reactions. The product could be liberated and the side protecting groups could be cleaved in one step by using TFA in CH_2Cl_2 (30 %, 1 h). The established PAA synthesis was fully compatible with standard peptide synthesis techniques. Therefore, amino acids or peptide sequences could be incorporated to introduce primary amine functionalities by using lysine (Lys) as a building block. By following established routes towards PEO–peptide conjugates, PEO–PAA conjugates could be obtained by using PEO-attached (PAP) resins.

PEO–*t*PAA (I) conjugates: **PEO-*block*-(Suc-Damp)$_{10}$**: ^{1}H NMR ([D$_6$]DMSO, 100 °C): $\delta=1.74$–1.98 (m, 10 H, β-C*H*-amine), 2.21–2.41 (m, 10 H, β-C*H*-amine), 2.67–3.30 (m, 70 H, α-CH_3-amine, α-CH_2-amine), 3.36–3.84 ppm (m, 344 H, O-CH_2-CH_2, O=C-CH_2-CH_2, α-CH_2-amide, β-CH_2-amid); ^{13}C NMR ([D$_6$]DMSO): $\delta=24.3$ (β-CH_2-amine), 31.0 (O=C-CH_2-CH_2, α-CH_3-amine), 36.2 (α-CH_2 amide), 53.3 (α-CH_3-amine, α-CH_2-amine), 60.1 (HO-CH_2), 69.9 (O-CH_2-CH_2), 171.7 ppm (*C*=O); FTIR: $\nu=1651$ (amide I), 1555 (amide II), 1103 (ether), 963 cm^{-1} (amine); MALDI-TOF MS: *m*/*z*: calcd for $C_{250}H_{493}O_{90}N_{31}$: 5373.77; found: 5450.67 $[M+2K]^+$.

PEO–*tp*PAA (II) conjugates: **PEO-*block*-Lys-(Suc-Damp-Lys$_2$)$_5$**: ^{1}H NMR ([D$_6$]DMSO, 100 °C): $\delta=1.23$–1.46 (m, 22 H, β-CH_2-lysine), 1.48–1.64 (m, 22 H, γ-CH_2 lysine), 1.64–1.90 (m, 22 H, α-CH_2 lysine), 2.28–2.43 (m, 20 H, β-CH_2-amine), 2.62–2.75 (m, 22 H, δ-CH_2 lysine), 2.75–2.85 (m, 15 H, α-CH_3-amine), 2.92–3.31 (m, 31 H, α-CH_2-amide), 3.40–3.74 (m, 20 H, α-CH_2-amide), 3.80–4.25 (m, O=C-CH_2-CH_2, O=C-(N*H*), O-CH_2-CH_2 PEO), 7.50–8.15 ppm (m, NH_2); FTIR: $\nu=1642$ (amide I), 1536 (amide II), 1171 (ether), 1132 cm^{-1}) (amine); MALDI-TOF MS: *m*/*z*: calcd for $C_{251}H_{504}O_{87}N_{38}$: 5468.93; found: 5490.03 $[M+Na]^+$.

PEO–*sp*PAA (III) conjugates: **PEO-*block*-Lys-(Suc-Spe-Lys$_2$)$_5$**: ^{1}H NMR ([D$_6$]DMSO, 100 °C): $\delta=1.22$–1.40 (m, 22 H, β-CH_2 lysine), 1.48–1.64 (m, 22 H, γ-CH_2 lysine), 1.64–1.74 (m, 22 H, α-CH_2 lysine), 2.24–2.40 (m, 20 H, β-CH_2-amine), 2.72–2.83 (m, 22 H, δ-CH_2 lysine), 2.87–2.99 (m, 20 H, β-CH_2-amine), 3.00–3.16 (m, 20 H, α-CH_2-amide), 3.16 −3.75 (m, 40 H, α-CH_2-amine, O=C-CH_2-CH_2, O=C-(N*H*), O-CH_2-CH_2-PEO), 7.50–8.00 ppm (m, NH_2); FTIR: $\nu=1780$ (amide I), 1653 (amide II), 1166 (ether), 1082 cm^{-1} (amine); MALDI-TOF MS: *m*/*z*: calcd for $C_{252}H_{504}O_{79}N_{43}$: 5400.98; found: 5402.60 $[M+H]^+$.

General procedure for the preparation of polyplexes: The used microfluidic device consisted of a Y-formed channel with a width of 400 μm. Due to this channel design, no turbulent mixing occurred. Instead, ion complex formation took place through diffusion of the two components at the interface of the solutions in the channel. Plasmid (0.1 mg mL^{-1}) and polymer solutions (0.6–2.0 mg mL^{-1}) were prepared in TRIS buffer (10 mM, pH 8.0) and filtrated by syringe filter (Nylon, 0.2 μm) to assure dust-free samples. The concentration of the solutions is not affected by this filtration as was shown by UV absorption measurements. The solutions are placed in syringes and pumped through the microfluidizer by using a syringe pump at a constant rate of 0.4 mL min^{-1}.

Characterization of the polyplexes with dynamic light scattering (DLS): Polyplex solutions (total DNA: 0.05 mg mL^{-1}) for DLS measurements were prepared by using the microfluidizer. To ensure clean preparation of the polyplex, the solutions were directly poured into a measuring cell.

Characterization of the polyplexes with AFM: Polyplexes at different N/P ratios were prepared by using the microfluidizer (solvent: HEPES buffer, 10 mM, pH 7.4) at a final concentration of 0.05 mg mL^{-1} DNA in the polyplex solution. After incubation for 30 min. the samples were prepared by spin coating (3000 rpm, 60 s), by using freshly cleaved mica substrate.

Ethidium bromide assay: Solutions of ethidium bromide (EB) (0.3 mg mL^{-1}), plasmid (0.016 mg mL^{-1}, 1 equiv(P) per mL) and the different polymer systems (10 equiv(N) per mL) in TRIS buffer (10 mM, pH 8.0) were prepared. Solutions of only EB (20 μL stock solution, 1980 μL buffer) and EB with plasmid (20 μL EB stock solution, 65 μL plasmid solution, 1915 μL buffer) were used as references. Polyplexes were prepared by mixing EB stock solution (20 μL) with plasmid solution (65 μL) and adding polymer solution (40 μL). After dilution with buffer to a total volume of 2 mL, fluorescence was measured at an excitation wavelength of $\lambda=480$ nm and an emission maximum of $\lambda=595$ nm.

Gel electrophoresis: For complex stability investigations an analytical agarose gel (0.8 %) was used. Agarose (4.0 g) was suspended in TAE buffer (pH 8.0) and heated in the microwave until it dissolved After cooling down to 60 °C, ethidium bromide solution was added to a final concentration of 10 μg L^{-1}. Afterwards, a gel was prepared (thickness about 4 mm). Plasmid (1.5 μg, 1 μg μL^{-1}) was dissolved in 10 mM Hepes buffer (25 μL, pH 7.4). In a separate tube, the adequate concentration of polymer was dissolved in a total volume of 10 mM Hepes buffer (25 μL, pH 7.4) to achieve N/P ratios of 2:1, 5:1, 10:1 and 50:1. The two solutions were mixed gently by pipetting up and down (no vortexing) and were incubated for 1 h. As a control, plasmid (1.5 μg, 1 μg μL^{-1}) was dissolved in Hepes buffer (50 μL, pH 7.4). Next, the polyplex solution (10 μL) was separated, mixed gently with 2.5 μL 6× DNA loading buffer, and stored at room temperature. Meanwhile, the remaining polyplex solution (40 μL) was digested with DNase (1 μL) for 15 min at 37 °C. The digestion was stopped with SDS loading buffer (10 μL 5×). A total volume of 12.5 μL for each experiment was applied in the slots of the agarose gel together with a 1 kb DNA ladder, and it was developed at 100 V for 30 min. Subsequently the gel was exposed to UV light ($\lambda=254$ nm) and the visible bands were analyzed.

Toxicity evaluation: Cell viability after transfection was determined on COS7 cells by quantitative analysis of the amount of ATP that was produced by metabolically active cells. CellTiter-Glo Luminescent Cell Viability Assay (Promega, Mannheim, Germany) was used. Cells were seeded in a 24-well cluster dish at a density of 10^4 cells 24 h prior to the experiments, and were cultivated in Dulbecco's Modified Eagle Medium that was supplemented with 10 % fetal calf serum. After 24 h in culture, the cells were washed with PBS (1 mL), and growth medium that con-

tained serum (400 μL) was added to the cells. The polyplexes (200 μL) were added to the cells. After incubation for 5 h at 37 °C (5 % (*v*/*v*) CO_2) the supernatants were removed, and the appropriate growth medium (1 mL) was added to each well. Thereafter, the cells were additionally cultured for a total of 48 h at 37 °C, 5 % (*v*/*v*) CO_2. Then the medium was replaced with Dulbecco's Modified Eagle Medium (1000 μL) that was supplemented with 10 % fetal calf serum and equivalent amounts of test reagent for 48 h. The reagent induced cell lyses, and generated a luminescent signal that was proportional to the amount of ATP that was present. After 2 min of mixing and 10 min of incubation at room temperature, the contents of the 24-well plates were transferred into 96-well plates, 3 values of 200 μL were obtained out of the 1000 μL content of a single well from the 24-well plate. The luminescent signal and the percentage of cell viability was calculated by comparing the appropriate luminescent signal to the signal that was obtained with non-transfected control cells.

Acknowledgements

Katharina Ostwald, Jessica Brandt, Anne Heilig, Heike Stephanowitz, Eberhard Krause, Birgit Schonert, Reinhard Siegel, Heidi Zastrow, Olaf Niemeyer, Margit Barth, Birgit Erhard and Erich C. are thanked for the contributions to this project. Financial support was received from the German Research Foundation through the Emmy Noether Program (BO 1762/2-3), the VW Foundation and the Max Planck Society.

[1] R. Duncan, H. Ringsdorf, R. Satchi-Fainaro, *J. Drug Targeting* **2006**, *14*, 337.
[2] a) J. B. Opalinska, A. M. Gewirtz, *Nat. Rev. Drug Discovery* **2002**, *1*, 503; b) F. D. Ledley, *Hum. Gene Ther.* **1995**, *6*, 1129.
[3] R. Duncan, *Nat. Rev. Drug Discovery* **2003**, *2*, 347.
[4] a) S. Akhtar, *Gene Ther.* **2006**, *13*, 739; b) R. Duncan, *Nat. Rev. Drug Discovery* **2003**, *2*, 347; c) W. T. Godbey, A. G. Mikos, *J. Controlled Release* **2001**, *72*, 115.
[5] a) A. C. Hunter, S. M. Moghimi, *Drug Discovery Today* **2002**, *7*, 998; b) V. Labhasetwar, *Curr. Opin. Biotechnol.* **2005**, *16*, 674; c) D. W. Pack, A. S. Hoffman, S. Pun, P. S. Stayton, *Nat. Rev. Drug Discovery* **2005**, *4*, 581; d) D. G. Anderson, D. M. Lynn, R. Langer, *Angew. Chem.* **2003**, *115*, 3261; *Angew. Chem. Int. Ed.* **2003**, *42*, 3153.
[6] E. Wagner, J. Kloeckner, in *Polymer Therapeutics I: Polymers As Drugs, Conjugates And Gene Delivery Systems, Vol. 192* (Eds.: R. Satchi-Fainaro, R. Duncan), Springer, Berlin, **2006**, pp. 135.
[7] M. X. Tang, F. C. Szoka, *Gene Ther.* **1997**, *4*, 823.
[8] O. Boussif, F. Lezoualch, M. A. Zanta, M. D. Mergny, D. Scherman, B. Demeneix, J. P. Behr, *Proc. Natl. Acad. Sci. USA* **1995**, *92*, 7297.
[9] a) M. Breunig, U. Lungwitz, R. Liebl, C. Fontanari, J. Klar, A. Kurtz, T. Blunk, A. Goepferich, *J. Gene Med.* **2005**, *7*, 1287; b) U. Lungwitz, M. Breunig, T. Blunk, A. Gopferich, *Eur. J. Pharm. Biopharm.* **2005**, *60*, 247; c) M. Neu, D. Fischer, T. Kissel, *J. Gene Med.* **2005**, *7*, 992; d) Y. Liu, D. C. Wu, W. D. Zhang, X. Jiang, C. B. He, T. S. Chung, S. H. Goh, K. W. Leong, *Angew. Chem.* **2005**, *117*, 4860; *Angew. Chem. Int. Ed.* **2005**, *44*, 4782.
[10] W. T. Godbey, K. K. Wu, A. G. Mikos, *J. Controlled Release* **1999**, *60*, 149.
[11] K. von Gersdorff, N. N. Sanders, R. Vandenbroucke, S. C. De Smedt, E. Wagner, M. Ogris, *Mol. Ther.* **2006**, *14*, 745.
[12] a) S. Boeckle, K. von Gersdorff, S. van der Piepen, C. Culmsee, E. Wagner, M. Ogris, *J. Gene Med.* **2004**, *6*, 1102; b) S. Choosakoonkriang, B. A. Lobo, G. S. Koe, J. G. Koe, C. R. Middaugh, *J. Pharm. Sci.* **2003**, *92*, 1710.
[13] a) R. Duncan, L. Izzo, *Adv. Drug Delivery Rev.* **2005**, *57*, 2215; b) M. J. Liu, J. M. J. Frechet, *Pharm. Sci. Technol. Today* **1999**, *2*, 393; c) S. E. Stiriba, H. Frey, R. Haag, *Angew. Chem.* **2002**, *114*, 1385; d) J. F. Bermejo, P. Ortega, L. Chonco, R. Eritja, R. Samaniego, M. Mullner, E. de Jesus, F. J. de la Mata, J. C. Flores, R. Gomez, A. Munoz-Fernandez, *Chem. Eur. J.* **2007**, *13*, 483; e) M. J. Liu, K. Kono, J. M. J. Frechet, *J. Controlled Release* **2000**, *65*, 121; f) R. Haag, *Angew. Chem.* **2004**, *116*, 280; *Angew. Chem. Int. Ed.* **2004**, *43*, 278.
[14] a) H. Petersen, K. Kunath, T. Kissel, A. L. Martin, S. Stolnik, C. J. Roberts, M. C. Davies, *J. Controlled Release* **2003**, *87*, 286; b) F. P. Seib, A. T. Jones, R. Duncan, *J. Controlled Release* **2007**, *117*, 291; c) D. Joester, M. Losson, R. Pugin, H. Heinzelmann, E. Walter, H. P. Merkle, F. Diederich, *Angew. Chem.* **2003**, *115*, 1524; *Angew. Chem. Int. Ed.* **2003**, *42*, 1486.
[15] H. G. Börner, H. Schlaad, *Soft Matter* **2007**, *3*, 394.
[16] L. Hartmann, E. Krause, M. Antonietti, H. G. Borner, *Biomacromolecules* **2006**, *7*, 1239.
[17] L. Hartmann, S. Häfele, R. Peschka-Suess, M. Antonietti, H. G. Börner, *Macromolecules* **2007**, *40*, 7771.
[18] W. Rapp, *Combinatorial Peptide and Nonpeptide Libraries*, VCH, Weinheim, **1996**.
[19] J.-F. Lutz, H. G. Börner, *Prog. Polym. Sci.* **2008**, *33*, 1.
[20] M. X. Tang, C. T. Redemann, F. C. Szoka, *Bioconjugate Chem.* **1996**, *7*, 703; J. Haensler, F. C. Szoka, *Bioconjugate Chem.* **1993**, *4*, 372.
[21] a) J. M. Harris, R. B. Chess, *Nat. Rev. Drug Discovery* **2003**, *2*, 214; b) G. Pasut, F. M. Veronese, in *Polymer Therapeutics I: Polymers As Drugs, Conjugates And Gene Delivery Systems, Vol. 192* (Eds.: R. Satchi-Fainaro, R. Duncan), Springer, Berlin, **2006**, pp. 95.
[22] D. Fischer, B. Osburg, H. Petersen, T. Kissel, U. Bickel, *Drug Metab. Dispos.* **2004**, *32*, 983.
[23] V. Hessel, H. Lowe, F. Schonfeld, *Chem. Eng. Sci.* **2005**, *60*, 2479.
[24] A. V. Kabanov, V. A. Kabanov, *Bioconjugate Chem.* **1995**, *6*, 7.
[25] S. V. Vinogradov, T. K. Bronich, A. V. Kabanov, *Bioconjugate Chem.* **1998**, *9*, 805.
[26] V. A. Bloomfield, *Curr. Opin. Struct. Biol.* **1996**, *6*, 334.
[27] P. C. Griffiths, A. Paul, Z. Khayat, K. W. Wan, S. M. King, I. Grillo, R. Schweins, P. Ferruti, J. Franchini, R. Duncan, *Biomacromolecules* **2004**, *5*, 1422.
[28] J. Kloeckner, E. Wagner, M. Ogris, *Eur. J. Pharm. Sci.* **2006**, *29*, 414.
[29] a) R. Golan, L. I. Pietrasanta, W. Hsieh, H. G. Hansma, *Biochemistry* **1999**, *38*, 14069; b) H. G. Hansma, R. Golan, W. Hsieh, C. P. Lollo, P. Mullen-Ley, D. Kwoh, *Nucleic Acids Res.* **1998**, *26*, 2481.
[30] S. W. Provencher, *Comput. Phys. Commun.* **1982**, *27*, 229.

Received: August 7, 2007
Revised: November 30, 2007
Published online: February 7, 2008

